Chapter 4

Accelerators and collider experiments

This chapter gives an introduction to particle accelerators and detectors as well as to data analysis tools relevant in this context. This involves the definition and application of concepts based on the kinematics developed in Chap. 2. Basic principles of particle accelerators are discussed as well as fixed target and beam collider experiments. The concepts of center of mass energy, luminosity, cross section, and event rates are introduced, followed by the basic building blocks of particle physics experiments. In order to be able to analyze the data gathered with collider experiments, we will introduce the concepts of rapidity, transverse and missing momentum (applications of momentum conservation) and invariant mass.

Modern techniques in experimental particle physics can be classified according to their use of accelerators. Non-accelerator-based experiments (e. g. the setup in Fig. 4.1) include measurements based on cosmic rays, solar and atmospheric neutrinos, and searches for dark matter. The latter, together with dark energy, could account for 95% of the universe. In the case of cosmic rays we can study high energy particles without having to accelerate them. Advances in neutrino physics have been achieved using large targets of (heavy) water surrounded by photomultipliers (e. g. Super-Kamiokande: neutrino oscillations). Accelerator-based experiments, on the other hand, include fixed target experiments and particle colliders, which are the topic of this chapter. As an example for particle colliders, the Large Hadron Collider (LHC) is shown in Fig. 4.2 with its four collision sites.

4.1 Particle accelerators: motivations

Particle accelerators are a fundamental tool for research in physics. Their importance and fields of use can be understood when one considers their main parameter, the beam energy. If we intend to use accelerators as large "microscopes", the spatial resolution increases with beam energy. According to the de Broglie equation, the relation between

Figure 4.1: *Example of a non-accelerator-based experiment.* Heavy water targets can be protected from radiation background by installing them in deep-underground facilities. The target is surrounded by photomultipliers.

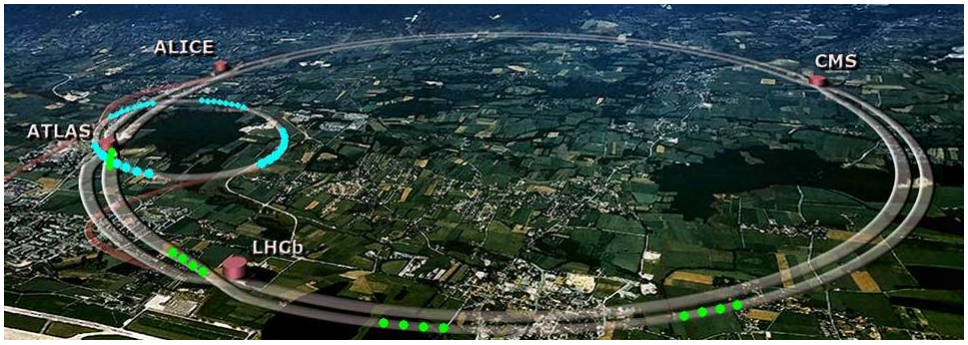

Figure 4.2: *The Large Hadron Collider at CERN with its four experiments CMS, ATLAS, LHCb, and ALICE.*

momentum $|\vec{p}|$ and wavelength λ of a wave packet is given by

$$\lambda = \frac{h}{|\vec{p}|}. \tag{4.1}$$

Therefore, larger momenta correspond to shorter wavelengths and access to smaller structures. In addition, it is possible to use accelerators to produce new particles. As we have seen in Chap. 2, this requires the more energy the heavier the particles are. Because beams are circulated for several hours accelerators are based on beams of stable particles and antiparticles, such as e^+, e^- or $p, \bar{p}$ or e, p (Deutsches Elektronen-Synchrotron, DESY). There are two possibilities as to what to collide a beam of accelerated particles with:

1. collision with another beam;
2. collision with a fixed target.

In both cases one can study the resulting interactions with particle detectors. By using a fixed target, one can furthermore produce a beam of secondary particles that may be stable, unstable, charged or neutral, solving the impossibility of accelerating unstable or neutral particles directly.

In the search for new sub-structures, Eq. (4.1) is the fundamental relation. It tells us that the resolution increases as we go to higher energies. For instance the resolution of 1 GeV/c and 10^3 GeV/c are:

$$|\vec{p}| = 1\,\frac{\text{GeV}}{\text{c}} \rightarrow \lambda = 1.24 \cdot 10^{-15}\,\text{m} \simeq \text{size of a proton}$$
$$|\vec{p}| = 10^3\,\frac{\text{GeV}}{\text{c}} \rightarrow \lambda = 1.24 \cdot 10^{-18}\,\text{m} \simeq \text{size of proton substructures, e. g. quarks.}$$

Consider now the second scenario mentioned above, namely the search for new particles with high mass. For a collision of a particle with mass m_1 and momentum $\vec{p}_1$ with another particle m_2, $\vec{p}_2$ the energy in the laboratory frame is given by[1]

$$\begin{aligned} E_L &= \sqrt{\vec{p}_1^{\,2}c^2 + m_1^2c^4} + \sqrt{\vec{p}_2^{\,2}c^2 + m_2^2c^4} \\ |\vec{p}_L| &= |\vec{p}_1 + \vec{p}_2| \\ E_L^2 - \vec{p}_L^{\,2}c^2 &= E^{*2} - \underbrace{\vec{p}^{\,*2}}_{=0}c^2 \\ \Rightarrow E^* &= \sqrt{E_L^2 - \vec{p}_L^{\,2}c^2}. \end{aligned}$$

The production energy threshold for particles produced at rest is therefore:

$$E^* = \sum_i m_i c^2, \text{ while } E_{\text{kin}} = 0$$

[1] Recall that we asterisk quantities given in the center of mass frame. See Sect. 2.2 for labeling conventions.

where m_i is the mass of the i-th particle of the final state. We can conclude that, since the center of mass energy E^* grows with the energy in the laboratory frame E_L, we can produce higher masses if we have higher energies at our disposal. This allows to produce particles not contained in ordinary matter.

Example: As an example, consider inelastic proton collisions. Imagine we want to produce three protons and one antiproton by colliding a proton beam against a proton target (e. g. a hydrogen target). The corresponding reaction is

$$pp \to \bar{p}ppp$$

where conservation of the baryon number requires the presence of one antiproton in the final state. What is the minimum momentum of the proton beam for the reaction to take place? Since particles and antiparticles have the same mass and the target is at rest in the laboratory frame, we find

$$\begin{aligned} m_1 = m_2 = m &= 0.9383\,\frac{\mathrm{GeV}}{\mathrm{c}^2} \\ |\vec{p}_L| = |\vec{p}_1|,\ |\vec{p}_2| &= 0 \\ \text{at threshold: } E^* &= 4mc^2 = 3.7532\,\mathrm{GeV} \\ \Rightarrow |\vec{p}_1| &= 6.5\,\frac{\mathrm{GeV}}{\mathrm{c}}. \end{aligned}$$

4.1.1 Center of mass energy

As we have seen, the center of mass energy E^* is the energy available in collision experiments. We therefore want to compare fixed target and colliding beam experiments concerning their available energy. In the case of beam-target collision, E^* is determined by (with m the mass of both the beam and target particles)

$$\begin{aligned} E_L &= \sqrt{\vec{p}_L^{\,2}c^2 + m^2c^4} + mc^2 \\ E^{*2} = M^2c^4 &= E_L^2 - \vec{p}_L^{\,2}c^2 = 2m^2c^4 + 2mc^2\sqrt{\vec{p}_L^{\,2}c^2 + m^2c^4}. \end{aligned}$$

Setting $|\vec{p}_L| = p_{\mathrm{inc}}$ and neglecting the mass of the target we get:

$$E^* = \sqrt{2mc^2 p_{\mathrm{inc}}c} = 1.37\,\sqrt{\mathrm{GeV}}\sqrt{p_{\mathrm{inc}}c} = 1.37\,\sqrt{\mathrm{GeV}}\sqrt{E_{\mathrm{inc}}}.$$

This means that, in the case of a fixed target experiment, the center of mass energy grows only with square root of E_{inc} (see Fig. 4.3).

However, in beam-beam collisions, we find $E^* = E_{\mathrm{CM}} = 2E_{\mathrm{inc}}$. Therefore, it is much more efficient to use two beams in opposite directions, as the following examples demonstrate

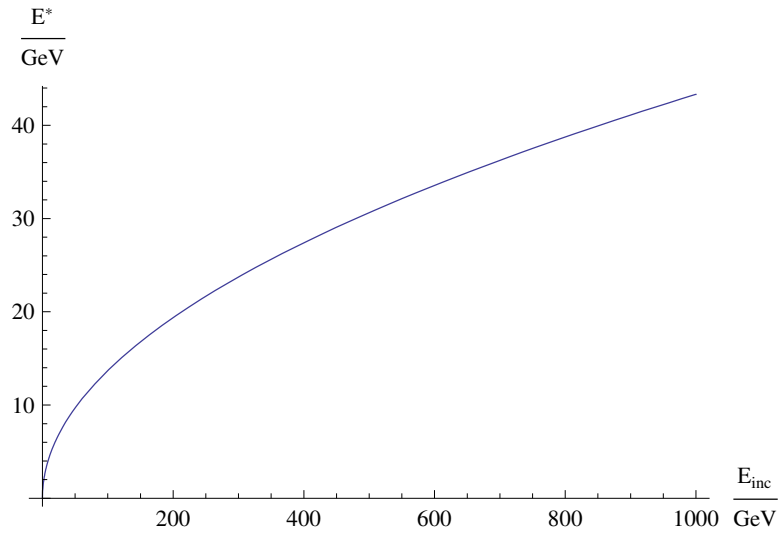

Figure 4.3: *Center of mass energy of the colliding beam for a fixed target experiment.* The energy increases with the square root of the beam energy.

(target is for instance hydrogen):

$$\overrightarrow{22\,\mathrm{GeV}} + \overleftarrow{22\,\mathrm{GeV}} \text{ has the same } E_{\mathrm{CM}} \text{ as } \overrightarrow{1\,\mathrm{TeV}} + m_{\mathrm{target}};$$
$$\overrightarrow{1\,\mathrm{TeV}} + \overleftarrow{1\,\mathrm{TeV}} \text{ has the same } E_{\mathrm{CM}} \text{ as } \overrightarrow{10^3\,\mathrm{TeV}} + m_{\mathrm{target}}.$$

The concept of colliding beams naturally leads to large circular accelerators. But for them to work properly some technical problems have to be solved. For instance, the particle density in a beam is much lower than in a solid or liquid target (see also the concept of luminosity in Sect. 4.3.2). Therefore, one tries to cross the beams many times and maximize the beam intensities (number of particle bunches per beam). As mentioned before, this approach only works with stable particles or antiparticles. Furthermore, in order to avoid beam-gas interactions (unintended fixed target collisions), a high vacuum is needed in the beam-pipe (about 10^{-9} Pa). Two beam lines are needed in the particle-particle case, whereas in the particle-antiparticle case one beam line is sufficient, with the two beams circulating in opposite directions. Finally, electronics represent another crucial part of the setup. At a rate of about $40 \cdot 10^6$ collisions per second a fast electronic system is necessary to decide what collisions to select.

4.2 Acceleration methods

Bearing in mind that an electric field $\vec{E}$ produces an accelerating force $\vec{F}$ on a charge q,

$$\vec{F} = q\vec{E},$$

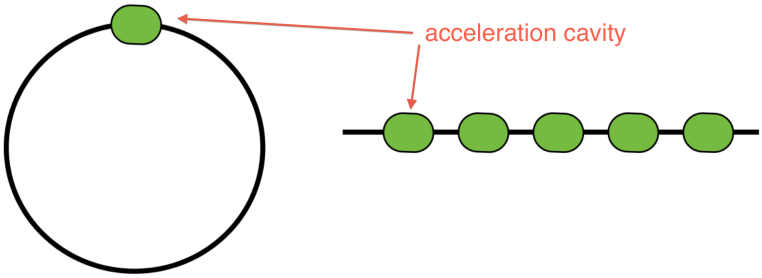

Figure 4.4: *Sketch of a circular (left) and linear (right) accelerator.* A circular machine needs to have one acceleration cavity, while a linear machine needs several cavities in series in order to reach high energies.

one could use an electrostatic field to accelerate charged particles. Since the maximal available potential difference (cf. Van de Graaff accelerator) is about 10 MV, one can accelerate particles up to 10 MeV. However, the fact that the electrostatic field is conservative ($\oint \vec{E} \cdot d\vec{l} = 0$) implies that the energy transfer only depends on the potential difference and not on the path. Therefore, circulating the beam in an electrostatic field does not lead to an increasing acceleration. The problem is solved by using several times a small but variable potential difference. This can be done using circular or linear machines. In a circular accelerator, one can use several times the same acceleration cavity (see Fig. 4.4, left), whereas in a linear accelerator several cavities in series are needed to reach high energies (see Fig. 4.4, right). In the case of a circular accelerator, the particles will receive a certain amount of energy at every turn, provided they are in phase with the accelerating potential. Because of the inertia principle, one further needs a magnetic field providing the centripetal force to keep particles on a circular path. An outline of historical developments in particle accelerators is given in Tab. 4.1. In the following sections, we will take a more detailed look at two types of accelerators: cyclotrons and synchrotrons.

4.2.1 Cyclotron

The sketch of a cyclotron is shown in Fig. 4.5. Particles are injected in the center and accelerated with a variable potential while a magnetic field $\vec{B}$ keeps them on spiral trajectories. Finally, particles are extracted and used in experiments. Cyclotrons are rather compact, as one can also see in Fig. 4.6. The maximal energy is of order 20 MeV for cyclotrons and up to 600 MeV for synchro-cyclotrons. For a particle moving in the cyclotron the centripetal and Lorentz forces are balanced:

$$m\frac{v^2}{\rho} = qvB \tag{4.2}$$

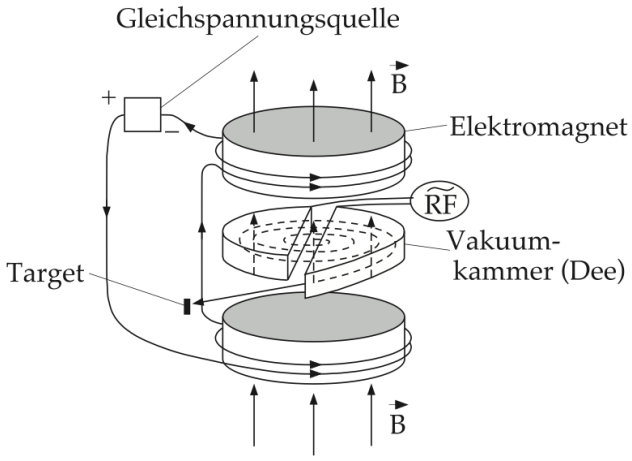

Figure 4.5: *Sketch of a cyclotron accelerator.* Source: [8, p. 108].

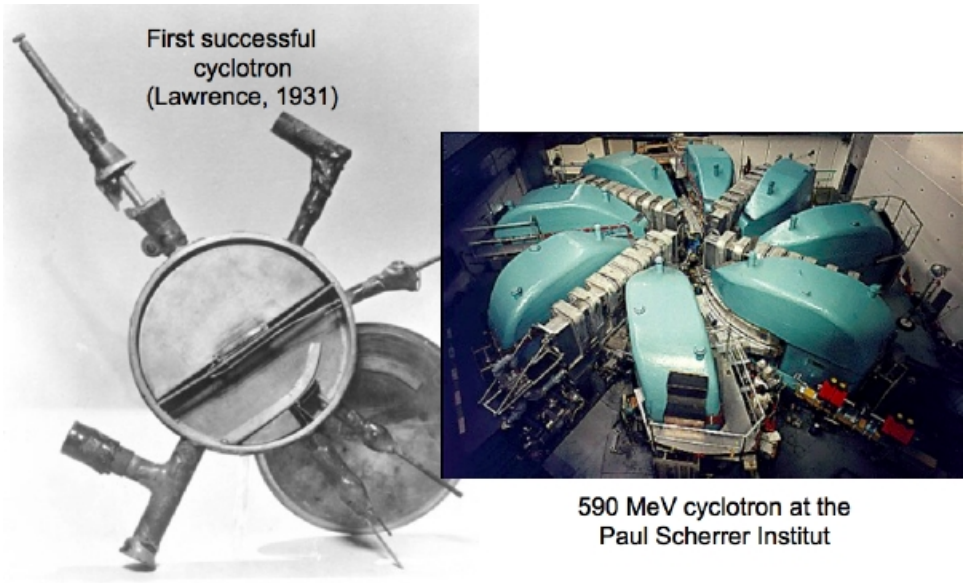

Figure 4.6: *A first prototype of a cyclotron (by Lawrence) and the* 590 MeV *isochronous cyclotron at PSI.*

Year	Accelerator	Beam energy
1921	"Kaskadengenerator" (Greinacher)	
1924–1928	Concept and first prototype of linear accelerator (Ising / Wideröe)	
1932	First nuclear reaction induced by cascade particle accelerator, $p^7\mathrm{Li} \rightarrow 2\alpha$ (Cockroft / Walton)	400 keV protons
1930	First Van de Graaff accelerator	1.5 MV
1930–1932	First cyclotron (concept: Lawrence)	1.5 MeV
	Upgraded cyclotrons (Synchrocyclotron)	$300 - 700$ MeV
1953	First synchrotron at Brookhaven lab—Cosmotron (concept: Oliphant / Veksler / McMillan)	3 GeV
1958	Proton Syncrotron (CERN)	28 GeV
1983	Tevatron (Fermilab)	1000 GeV
1990	HERA (DESY): first and only electron-proton collider	
2008	Large Hadron Collider (CERN)	up to 7000 GeV

Table 4.1: Evolution timeline in particle accelerators (q. v. [7, pp. 9]).

where v is the velocity of the particle, m the mass, q the charge, and ρ the trajectory radius. This yields for the cyclotron frequency ω

$$v = \omega\rho \tag{4.3}$$

$$\Rightarrow \omega = \frac{qB}{m}. \tag{4.4}$$

The alternating high voltage used to accelerate the particles (see Fig. 4.5) matches the cyclotron frequency, such that the particles are accelerated when passing the capacitor between the two half disks, also called as "D's". We can also conclude that the radius of the particle trajectory grows linearly with its momentum. For relativistic particles, Eq. (4.4) has to be modified:

$$\omega' = \frac{qB}{\gamma m}$$

where $\gamma = 1/\sqrt{1 - v^2/c^2}$. This modification has, for example, the following effect on the revolution frequency:

$$\frac{v}{c} = 50\% \Rightarrow \gamma = 1.155 \Rightarrow \omega' = 0.86\omega$$
$$\frac{v}{c} = 99\% \Rightarrow \gamma = 7.1 \Rightarrow \omega' = 0.14\omega.$$

Isochronous cyclotrons compensate for the variation in frequency by increasing the magnetic field (rather than changing the frequency) with the radius.

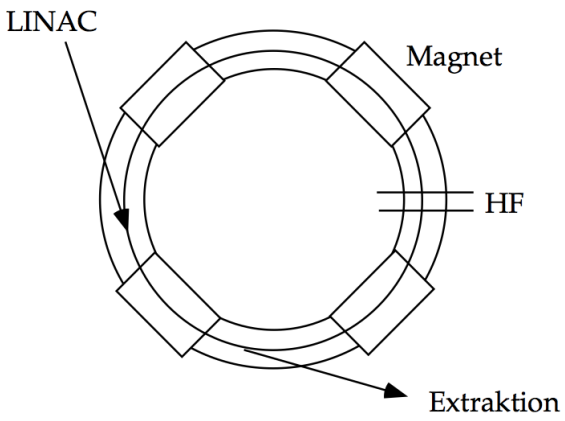

Figure 4.7: *Sketch of a synchrotron accelerator.* High frequency cavities are used to accelerate the particles. Dipole magnets keep them on circular trajectories. Linear accelerators are used for pre-acceleration and injection. Source: [8, p. 110].

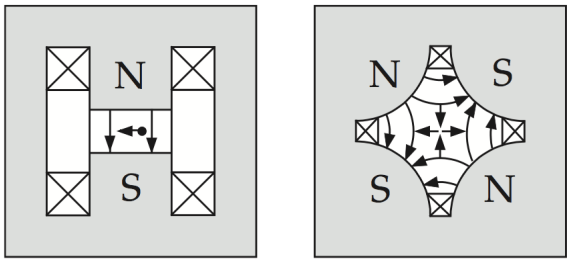

Figure 4.8: *Magnets used in synchrotrons.* Dipole magnets (left) keep the beam on a circular path, while quadrupole magnets (right) focus particles in the vertical or horizontal plane. Source: [8, p. 111].

4.2.2 Synchrotron

In the case of the synchrotron, the trajectory radius is kept constant. This is achieved by dipole magnets (see Fig. 4.8), while high frequency cavities are used to accelerate the particles (see Fig. 4.7). The problem of reducing the cross section to increase the particle density is solved by using quadrupole magnets (see Fig. 4.8). Their focussing and defocussing properties can be combined in a way as to lead to an overall focussing of the beam. Starting from Eq. (4.2), we have for the radius ρ

$$\rho = \frac{p}{qB}.$$

This yields, setting $q = ze$ (with e the unit charge),

$$cp[\text{eV}] = czB\rho = 3 \cdot 10^8 \frac{\text{m}}{\text{s}} zB[\text{T}]\rho[\text{m}] \tag{4.5}$$

$$\Rightarrow p\left[\frac{\text{GeV}}{\text{c}}\right] = 0.3zB[\text{T}]\rho[\text{m}] \tag{4.6}$$

for the momentum.

Example: As an example, we consider the LHC at CERN: With a circumference of 27 km, yielding a radius of 4.3 km, an average magnetic field of 5.4 T is needed to keep protons with momentum 7 TeV/c on circular trajectories. Magnetic fields of this magnitude require very large currents and therefore superconductors which only work at low temperatures (about 2° K). The superconducting cables are therefore cooled with liquid helium.

Particle beams are injected into the vacuum pipe at relatively low energy with the magnetic field at its minimal value. Because the particles traverse acceleration cavities at every turn, the momentum grows accordingly. Since the beam has to be kept on the same radius, the magnetic filed also has to grow. On the other hand, rising velocity means changing revolution frequency and the frequency of the potential differences must be kept in phase with the particles. When maximum momentum is reached the accelerating cavities are switched off and the beam can be extracted to be used in experimental areas (see Fig. 4.9) or to be injected in larger synchrotrons (see Fig. 4.10). If the beam remains in the synchrotron ring it can be steered to cross other beams in collision points.

Another possible application of synchrotrons is to use the synchrotron radiation emitted by circulating beams. For this purpose one uses electrons, since they produce more synchrotron radiation than hadrons because of their smaller mass. The highly energetic photons emitted are used for measurements in solid state physics and protein research. An example is the Swiss Light Source at the Paul Scherrer Institute (Villigen, Switzerland), where electrons are pre-accelerated by a 100 MeV linear accelerator, injected into a synchrotron of 288 m circumference, kept on track by 36 dipole magnets with 1.4 T field, focussed by 177 quadrupole magnets, for a total beam energy of 2.8 GeV.

4.3 Particle physics experiments

In the following sections we introduce or recapitulate some basic concepts in particle physics experiments.

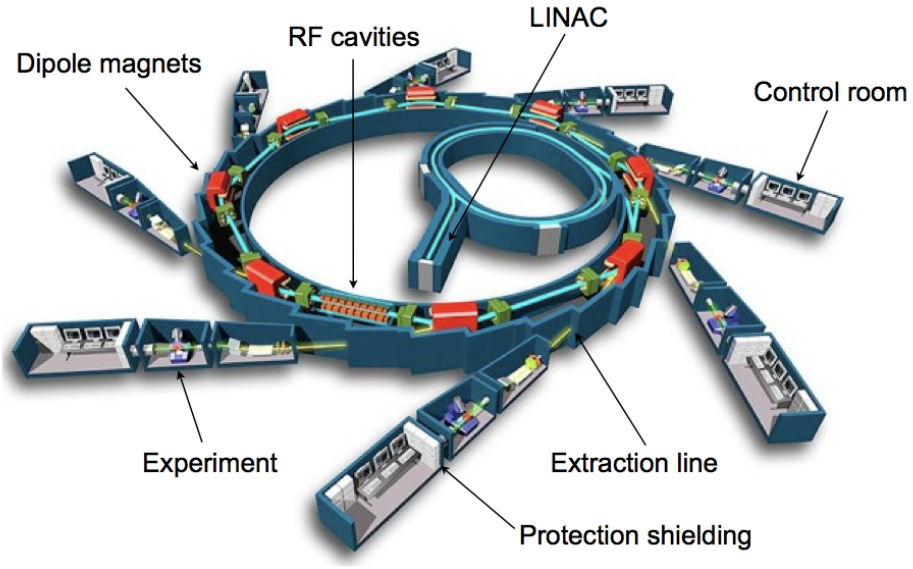

Figure 4.9: *Schematic view of a synchrotron.* Beams can be extracted and used in several experimental areas.

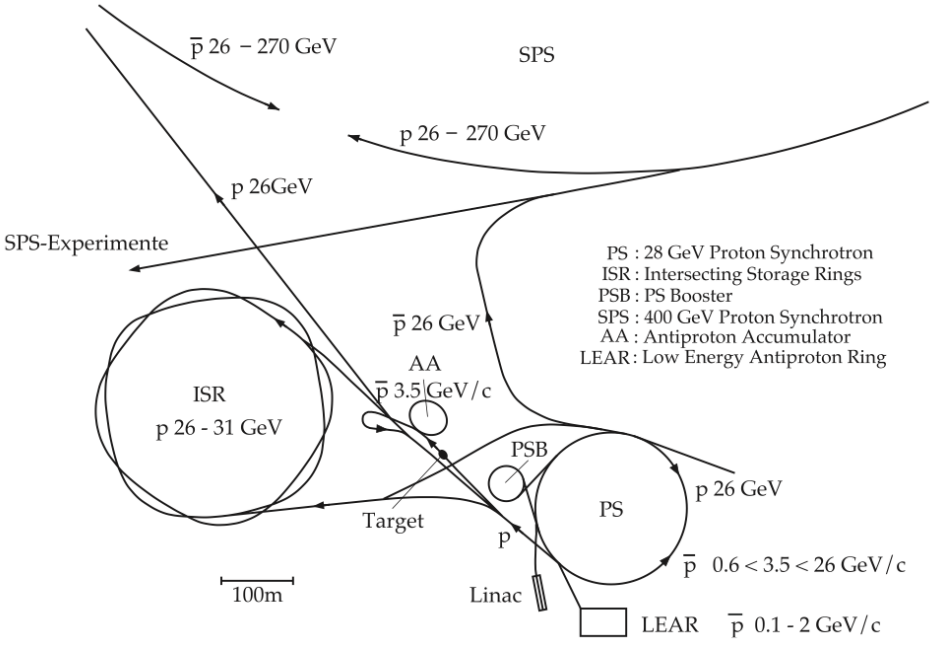

Figure 4.10: *Accelerator system at CERN.* Beams accelerated in linear machines and small synchrotrons are injected into larger synchrotron rings. Source: [8, p. 113].

4.3.1 Cross section

For a detailed introduction to the concept of cross section see Sect. 3.2.2. We recall that cross sections have dimension of area (cm^2). The common unit is barn, defined as

$$1\,\mathrm{b} = 10^{-24}\,\mathrm{cm}^2.$$

Until now, we have used the total cross section σ. This is a sum of contributions by many final states:

$$\sigma_{\mathrm{tot}} = \sum_i \sigma_i.$$

Example: Results of total cross section measurements for pp and $p\bar{p}$ collisions are shown in Fig. 4.11.

4.3.2 Luminosity

While cross sections characterize the scattering process, the luminosity characterizes an accelerators performance. With cross section σ and number of events per second R, the luminosity L is given by

$$R = L\sigma. \tag{4.7}$$

Because the dimension of the cross section is a surface, the units of luminosity are $\mathrm{cm}^{-2}\mathrm{s}^{-1}$.

The meaning of luminosity can be illustrated considering e. g. an e^+e^- accelerator with N particles per beam, revolving f times per second. We assume a Gaussian shaped beam with dimensions s_x and s_z, which yields a transverse size of $4\pi s_x s_z$. In one turn, one electron crosses $N/(4\pi s_x s_z)$ positrons. Because there are N particles revolving in each beam f times per second the number of collisions per second is

$$L = \frac{fN^2}{4\pi s_x s_z}. \tag{4.8}$$

From Eq. 4.7, the number of events per second is

$$R = \frac{\sigma f N^2}{4\pi s_x s_z}. \tag{4.9}$$

From Eq. (4.8) we notice that the luminosity can be increased by reducing the cross section of the beam, by increasing the number of particles in the beam or by increasing the revolution frequency.

In general, the luminosity of an accelerator gradually increases over time, while accelerator physicists learn how to operate the machine and to squeeze the beam size at the

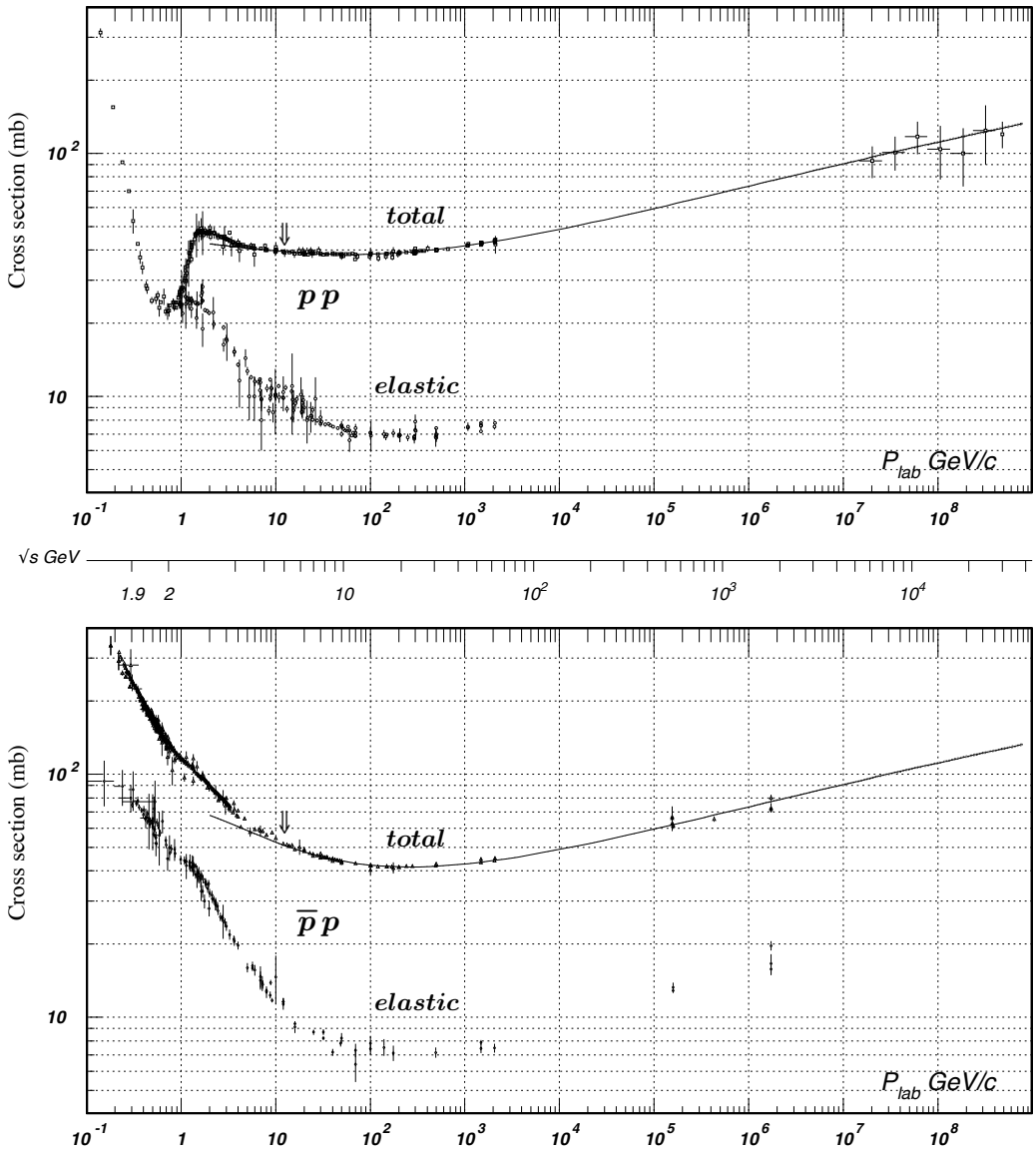

Figure 4.11: *Total and elastic cross sections for pp and $p\bar{p}$ collisions as a function of laboratory beam momentum and total center of mass energy.* Source: [9].

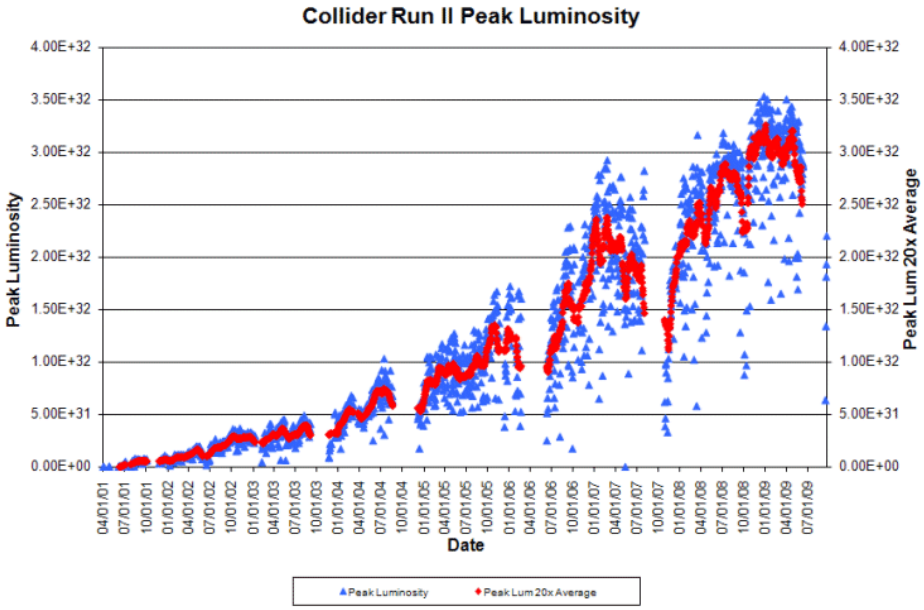

Figure 4.12: *Instantaneous luminosity at Tevatron as a function of time (2001 – 2009).* Note that the target luminosity for LHC is $10^{34}\,\mathrm{cm}^{-2}\mathrm{s}^{-1}$.

intersection point. For example, the evolution of instantaneous luminosity over time at Tevatron is shown in Fig. 4.12.

The integral of the delivered luminosity over time is called integrated luminosity and is a measure of the collected data size. The integrated luminosity delivered by Tevatron until early 2009 is shown in Fig. 4.13.

Example: Consider an accelerator ring with the following properties:

- Ring length $= 100\,\mathrm{m}$;
- Revolution frequency $= 3 \cdot 10^6\,\mathrm{Hz} = 3\,\mathrm{MHz}$;
- $N = 10^{10}$ particles;
- $s_x = 0.1\,\mathrm{cm}$, $s_z = 0.01\,\mathrm{cm}$.

Using Eq. (4.9), we can calculate $L = 10^{29}\,\mathrm{cm}^{-2}\mathrm{s}^{-1}$. If we are interested in a rare process, for example $e^+e^- \to p\bar{p}$ (the cross section is $\sigma = 1\,\mathrm{nb} = 10^{-33}\,\mathrm{cm}^2$) and have $E_{\mathrm{CM}} \sim 2 - 3\,\mathrm{GeV}$ we only expect $R = 10^{-4}$ events per second or about 0.35 events per hour.

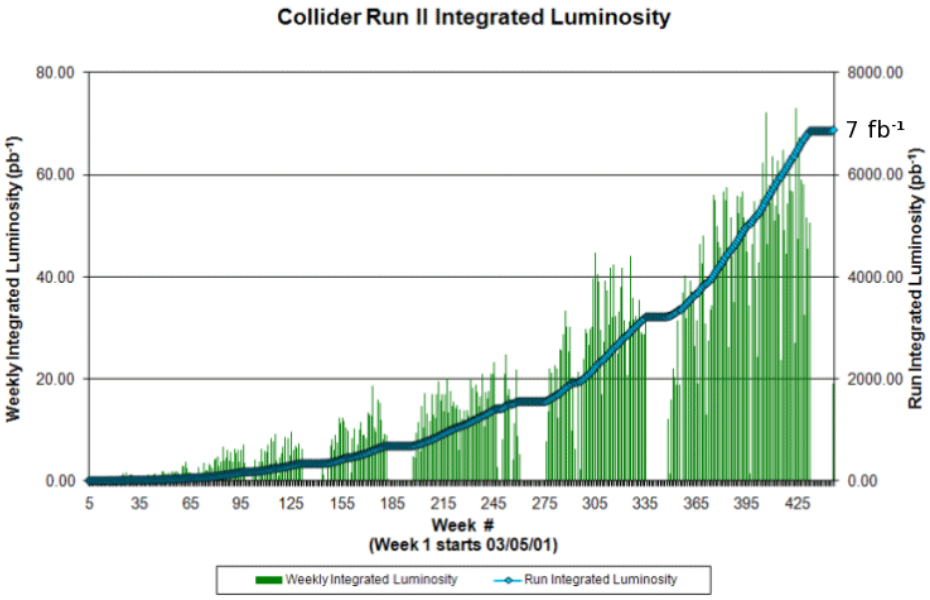

Figure 4.13: *Integrated luminosity at Tevatron as function of time.*

4.3.3 Particle detectors

To gather data from experiments carried out at accelerators, we need particle detectors. They are disposed around the interaction region and detect (directly or indirectly) the reaction products. Typically, the following measurements are performed on final state particles:

- Spatial coordinates and timing of final state;
- Momentum;
- Energy;
- Type of particle (particle ID).

Because of kinematical constraints, for fixed target experiments the production of final states is mainly in the forward direction. Therefore, the detector has to cover only a small solid angle (see Fig. 4.14). In colliding beam experiments, on the other hand, cylindrically symmetric detectors with ermeticity down to small angles are preferred (see Fig. 4.15). A collider physics experiment has in general tracking detectors in a solenoidal field surrounded by calorimeters and particle ID detectors (e. g. muon ID). To allow the momentum measurements, a solenoidal magnetic field is applied parallel to the colliding beams. The particles trajectories in the magnetic field are measured in the inner layers by silicon pixel and silicon strip tracking devices. They are surrounded by calorimeters measuring

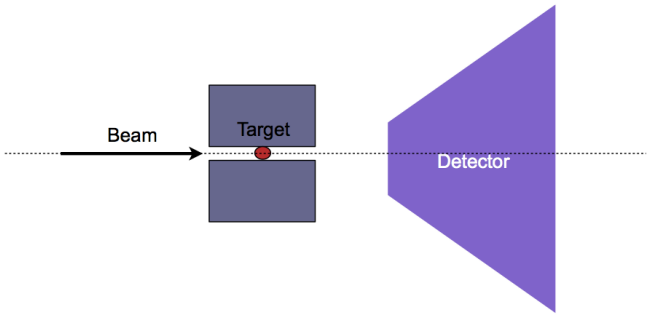

Figure 4.14: *Schematic view of an experimental setup for a fixed target experiment.*

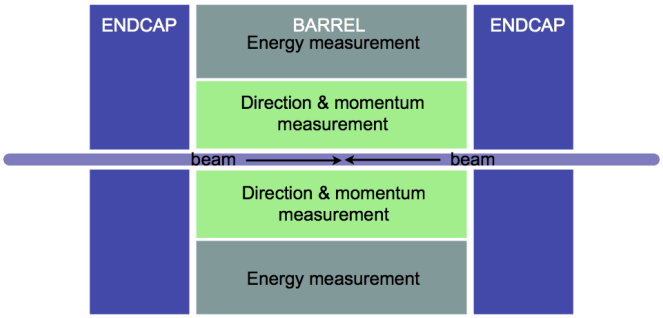

Figure 4.15: *Schematic view of a detector for colliding beam experiments.*

the particles' energy. The general structure of such a detector, shown in Fig. 4.15, is also visible in the Compact Muon Solenoid (CMS) experiment at LHC. A sketch of the CMS experiment is given in Fig. 4.16.

In high energy experiments the momentum measurement is based on the deflection of charged particles in a magnetic field. Consider a simple case involving a dipole magnet (Fig. 4.17(a)). One can measure the track direction before and after the bending influence of the magnetic field to obtain the angle θ. The momentum is derived from Eq. (4.6):

$$
\begin{aligned}
p &= 0.3BR \\
\text{length} = l &= 2R \sin\left(\frac{\theta}{2}\right) \sim R\theta \\
\Rightarrow \theta &= \frac{\text{length}}{R} = \frac{0.3Bl}{p} \\
\Rightarrow p &= \frac{0.3Bl}{\theta}.
\end{aligned}
$$

In collider experiments the B field is parallel to the beams, which means that curvature only happens in the transverse plane (Fig. 4.17(b)). The momentum resolution is given

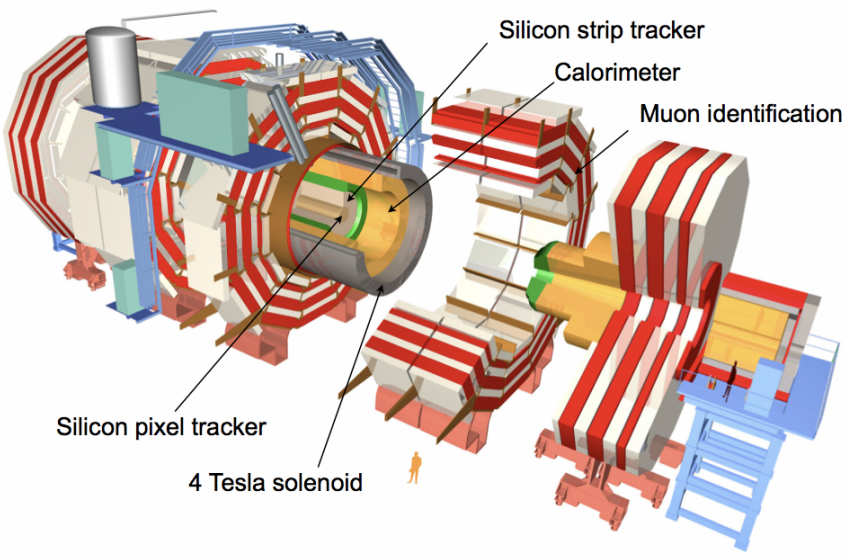

Figure 4.16: *The CMS experiment at the LHC.*

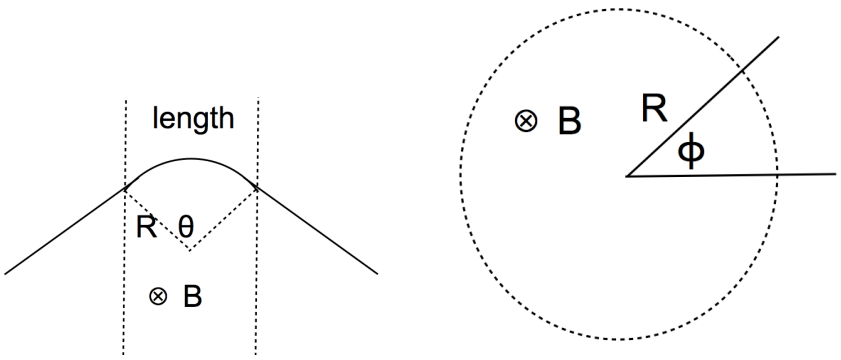

(a) (b)

Figure 4.17: *Momentum measurement in collider experiments using a magnetic field.* The magnetic field is parallel to the beams (orthogonal to the page).

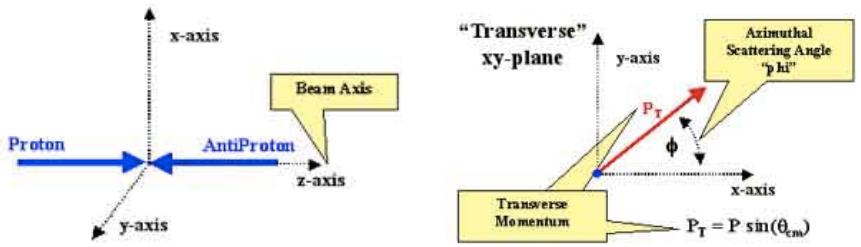

(a) (b)

Figure 4.18: *Axes labelling conventions (a) and definition of transverse momentum (b).* Source: [10].

by

$$\frac{\sigma(p_{\mathrm{T}})}{p_{\mathrm{T}}} = \frac{\sigma_{r\phi} p_{\mathrm{T}}}{0.3 B l_R^2} \left[\frac{720}{n+4}\right]^{-\frac{1}{2}}$$

where $\sigma_{r\phi}$ is the error on each measurement point, l_R the radial length of the track, and n the number of equidistant points.

4.4 Kinematics and data analysis methods

In this section we describe the data analysis tools used in collider particle physics experiments discussed in Sect. 4.3. We introduce variables in the laboratory frame and methods based on momentum conservation and invariant mass. Momentum conservation leads to the concepts of transverse momentum and missing mass. As examples, we discuss two- and three-jet events as well as the W boson discovery.

4.4.1 Pseudorapidity and transverse momentum

Consider the collision of two beams in the laboratory frame. The axes labelling conventions are given in Fig. 4.18(a) ($p\bar{p}$ scattering). The momentum of each particle produced in a collision can be decomposed in a component parallel to the beams (longitudinal, along the z direction) and one perpendicular to the beams (transverse, in the xy plane) as shown in Fig. 4.18(b). The transverse component of the momentum is given by ($\Theta^* \equiv \theta_{\mathrm{CM}}$)

$$p_{\mathrm{T}} = p \sin(\theta_{\mathrm{CM}})$$

and spans an angle ϕ with the x axis. To measure the longitudinal angle of the emerging particle jet one usually uses a variable called pseudorapidity η. It is defined by

$$\eta = -\ln\left[\tan\left(\frac{\theta_{\mathrm{CM}}}{2}\right)\right]$$

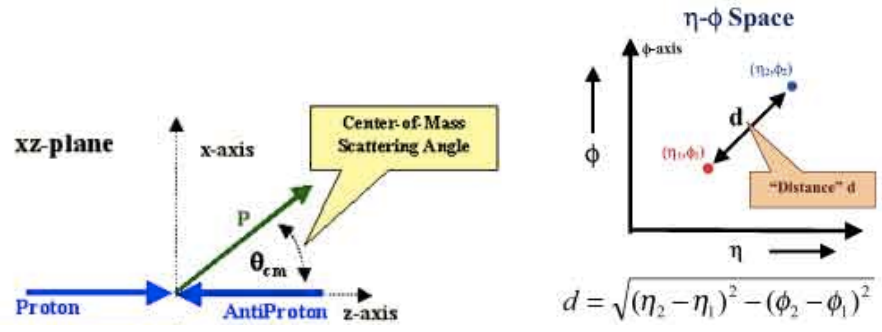

(a) (b)

Figure 4.19: *Definition of the longitudinal scattering angle θ_{CM} (a) and definition of particle distance in the η-ϕ plane (b).* Source: [10].

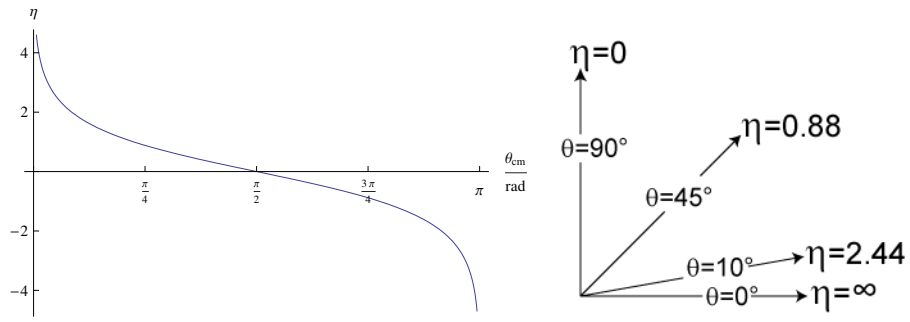

(a) (b)

Figure 4.20: *Pseudorapidity as a function of θ_{CM} (a) and pseudorapidity for various values of θ_{CM} (b).* Source (b): [11].

and is Lorentz invariant under longitudinal boosts (see Fig. 4.19(a)). Momenta in the transverse plane are also invariant under longitudinal relativistic transformations. Therefore, the distance between single particles or jets of particles is usually measured in the $\eta\phi$ plane, as shown in Fig. 4.19(b).

Particles produced at $\theta_{\mathrm{CM}} = 90°$ have zero pseudorapidity. As visualized by Fig. 4.20(a) and 4.20(b), high $|\eta|$ values are equivalent to very shallow scattering angles. Typical coverage of central detectors extends to $|\eta| \sim 3$. Coverage of high rapidities ($\theta_{\mathrm{CM}} < 5°$) can be achieved with detectors placed at large z positions.

4.4.2 Momentum conservation in particle jets

Experiments in hadron colliders usually deal with particles at high transverse momentum. This is because the incoming particles collide head-on and have no transverse momentum before scattering and therefore, the final state particles must have zero *total* transverse momentum. Processes involving large momentum transfer produce particles in the center

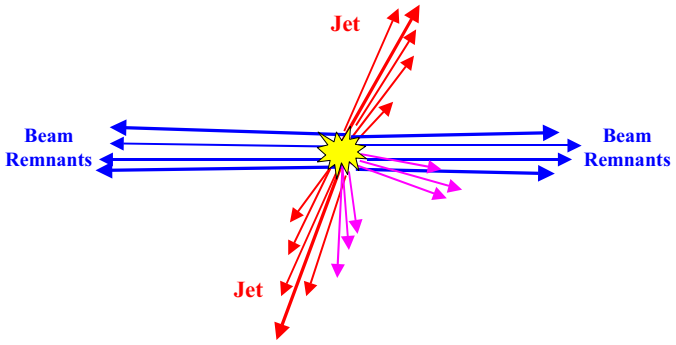

Figure 4.21: *Two jet event production at hadron colliders.* Source: [12].

of the detector (small pseudorapidity). An example of such a process is given in Fig. 4.21. The experimental signature of a two jet event is shown in Fig. 4.22. The calorimeter measures the deposited energy in cells of the η-ϕ plane. Both charged and neutral particles are detected. The histogram shows the energy measured in each cell. Note that the main signals are symmetric in azimuth and at about zero pseudorapidity. The momentum of each *charged* particle in a jet is measured by the central tracking chamber. Low momentum components yield smaller bending radii and the total transverse momentum has to be zero.

Electron-positron pairs can annihilate producing quark pairs (see Fig. 4.23(a)). This was studied for example at the Large Electron-Positron Collider (LEP). In some cases, a gluon can be radiated from one of the outgoing quarks (see Fig. 4.23(b)). In the latter case one observes three particle jets in the final state: two quark jets and one gluon jet. If no particle escapes the detector the three jets must have total transverse energy equal to zero. In the next section we discuss the case of particles escaping the experiment undetected. This topic is discussed more thoroughly in Chap. 8.

4.4.3 Missing mass method

A collision is characterized by an initial total energy and momentum ($E_{\rm in}$, $\vec{p}_{\rm in}$). In the final state we have n particles with total energy and momentum given by:

$$E = \sum_{i}^{n} E_i, \tag{4.10}$$

$$\vec{p} = \sum_{i}^{n} \vec{p}_i. \tag{4.11}$$

Sometimes an experiment may measure $E < E_{\rm in}$ and $\vec{p} \neq \vec{p}_{in}$. In this case one or more particles have not been detected. Typically this happens with neutral particles, most often neutrinos, but also with neutrons, π^0, or $K^0_{\rm L}$. The latter have a long lifetime and may decay outside the sensitive volume. To quantify this process, we introduce the concept of missing

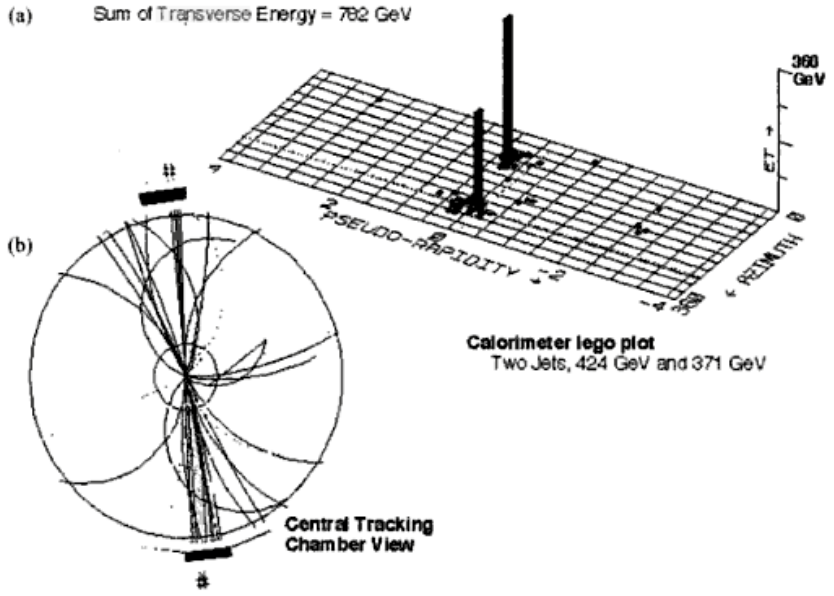

Figure 4.22: *Two jet event, reconstructed in the tracking chamber (b) and calorimeter signals (a) of the DØ experiment.*

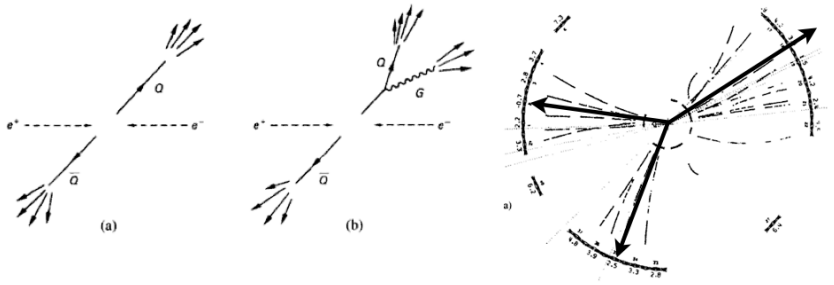

Figure 4.23: *Two- and three-jet events in e^+e^- collisions.* The rightmost sketch shows the tracks reconstructed in the central tracking detector.

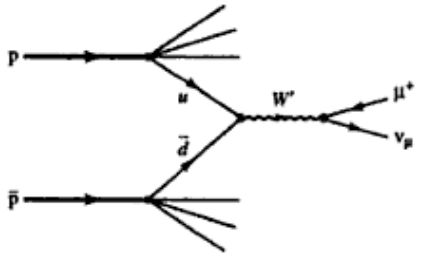

Figure 4.24: *Production and decay of a W^+ boson in a $p\bar{p}$ collision.*

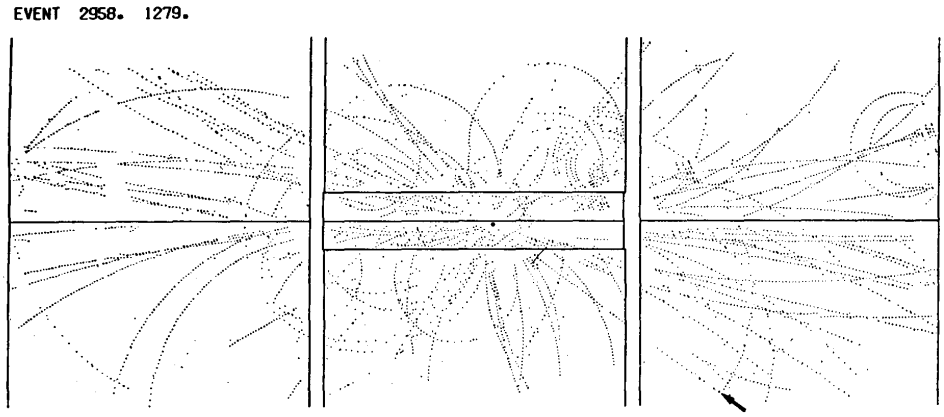

Figure 4.25: *Event with a W boson decay candidate via $W^+ \to e^+ + \nu_e$.* The event was recorded by the UA1 experiment (CERN). Source: [13, p. 112].

mass:

$$\text{missing mass} \times c^2 = \sqrt{(E_{\text{in}} - E)^2 - (\vec{p}_{\text{in}} - \vec{p})^2 c^2}. \tag{4.12}$$

The missing mass is measured for every collision and its spectrum is plotted. If the spectrum has a well-defined peak one particle has escaped our detector.

Example: Consider the decay of W bosons. They can be produced in proton-anti-proton collisions mainly via the process shown in Fig. 4.24; a u-quark collides with an anti-d-quark producing a W^+ boson. The W^+ then decays into a neutrino-lepton pair. The muon is detected and its momentum can be measured. The neutrino escapes the detector undetected. The total sum of the transverse momenta is therefore not zero! In other words, the experimental signature of the neutrino in the experiment is the *missing transverse momentum*. One of the first events [13, p. 112] attributed to production and decay of a W^+ boson is shown in Fig. 4.25. The arrow shows the lepton (e^+) and the missing momentum is compatible with the e^+ transverse momentum.

4.4.4 Invariant mass method

The invariant mass is a characteristic of the total energy and momentum of an object or a system of objects that is the same in all frames of reference. When the system as a whole is at rest, the invariant mass is equal to the total energy of the system divided by c^2. If the system is one particle, the invariant mass may also be called the rest mass:

$$m^2c^4 = E^2 - \vec{p}^2c^2.$$

For a system of N particles we have

$$W^2c^4 = \left(\sum_i^N E_i\right)^2 - \left(\sum_i^N \vec{p}_i c\right)^2 \tag{4.13}$$

where W is the invariant mass of the decaying particle. For a particle of Mass M decaying into two particles, $M \to 1+2$, Eq. 4.13 becomes:

$$M^2c^4 = (E_1+E_2)^2 - (\vec{p}_1+\vec{p}_2)^2c^2 = m_1^2c^4 + m_2^2c^4 + 2(E_1E_2 - \vec{p}_1\cdot\vec{p}_2c^2) = (p_1+p_2)^2.$$

Example: Particles like ρ, ω, ϕ have average lifetime of $10^{-22} - 10^{-23}$ s. How do we know of their existence if they live so shortly? Consider, for example, the reaction $pp \to pp\pi^+\pi^-$. We identify all four particles in the final state and measure their momentum. Let's focus on the pion pair, the total energy and momentum of the pair are:

$$E = E_+ + E_-$$
$$\vec{p} = \vec{p}_+ + \vec{p}_-.$$

The corresponding invariant mass is

$$Mc^2 = \sqrt{E^2 - \vec{p}^2c^2}.$$

The event distribution for the variable M will look like the plot in Fig. 4.26. The peak in the event rate at m_ρ is evidence for ρ production.

Example: Another example illustrating this point is the Z discovery in 1984. Fig. 4.27 shows an event where the Z boson, after production by proton-proton collision decays into an e^+e^- pair (white dashed lines). The invariant mass of the pair is about 92 GeV.

Example: Consider now the π^0 reconstruction. Neutral pions decay in photon pairs in about 99% of the cases. By measuring the angle and energy of the emitted photons (see Fig. 4.28) one can reconstruct the mass of the decaying pion (see Fig. 4.29).

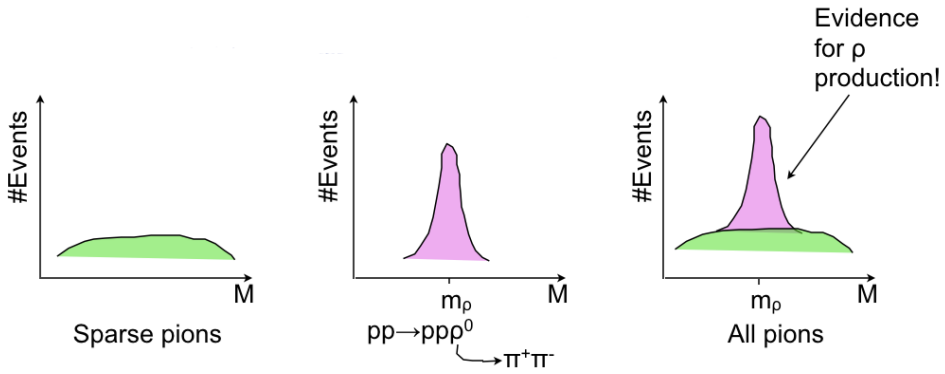

Figure 4.26: *Event distribution for invariant mass of the pion pair in the process* $pp \to pp\pi^+\pi^-$. The sparse pions' (left) distribution is broad and can be predicted using simulation techniques. The invariant mass of the pion pairs stemming from ρ^0 decay (center) is peaked around m_ρ. All pions contribute to the recorded events (right).

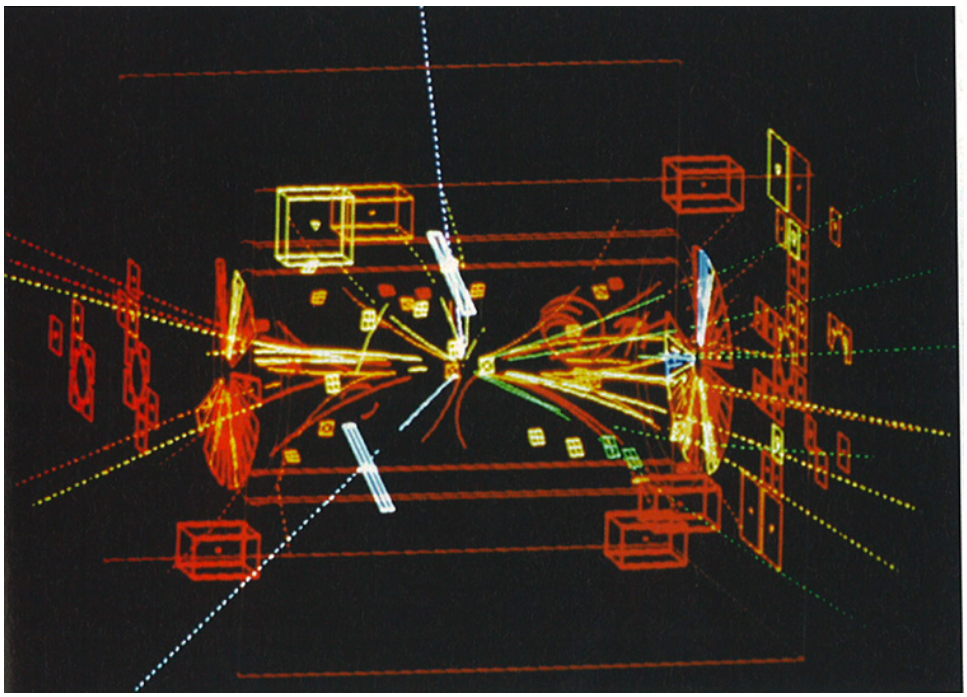

Figure 4.27: Z^0 *boson discovery at the UA2 experiment (CERN).* The Z^0 boson decays into a e^+e^- pair, shown as white dashed lines.

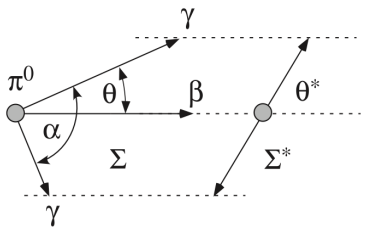

Figure 4.28: π^0 *decay in two photons.* Σ denotes the laboratory frame (left) and Σ^* denotes the pion rest frame (right). Source [8, p. 95].

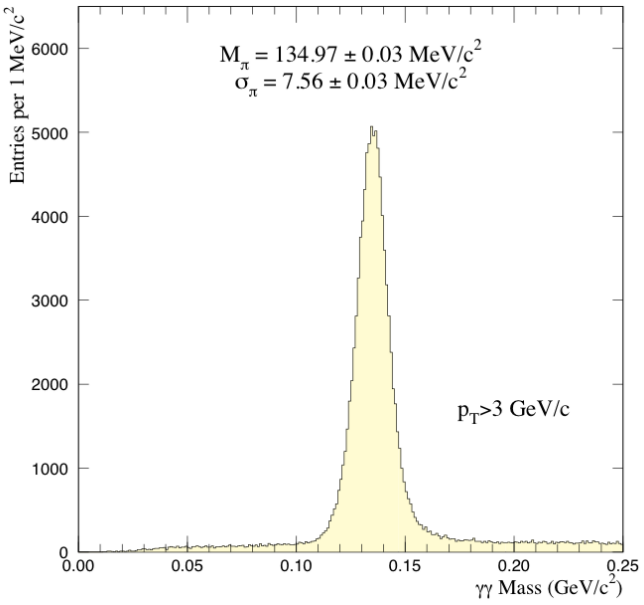

Figure 4.29: *Invariant mass spectrum for photon pairs.* The π^0 appears as a peak at the pion mass.

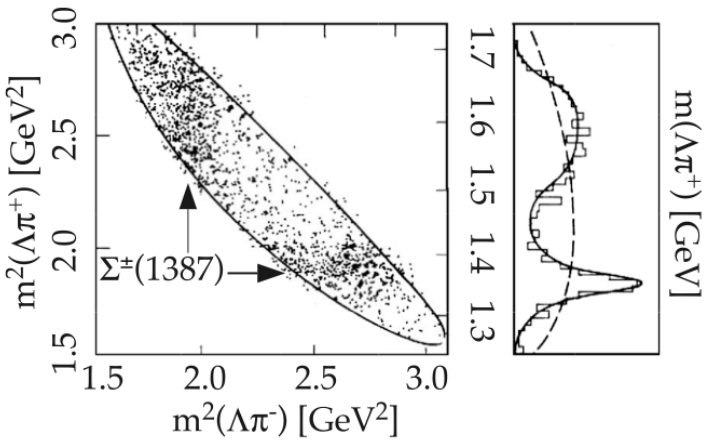

Figure 4.30: *Dalitz plot for* $K^- p \to \pi^+\pi^-\Lambda$ $(\Lambda \to \pi^- p)$. Source: [8, p. 200].

Example: In case of three body decays, $R \to 1 + 2 + 3$, one can define three invariant masses:

$$\begin{aligned} m_{12}^2 c^4 &\equiv (p_1 + p_2)^2 \\ m_{13}^2 c^4 &\equiv (p_1 + p_3)^2 \\ m_{23}^2 c^4 &\equiv (p_2 + p_3)^2. \end{aligned}$$

This yields

$$\begin{aligned} m_{12}^2 + m_{13}^2 + m_{23}^2 &= m_1^2 + m_2^2 + m_3^2 + (p_1 + p_2 + p_3)^2 \frac{1}{c^4} \\ &= m_1^2 + m_2^2 + m_3^2 + M^2. \end{aligned}$$

This means that there are only two independent invariant masses.

As an example, let's study the reaction:

$$K^- p \to \Lambda\pi^+\pi^- \ (\Lambda \to \pi^- p).$$

We can measure two invariant masses:

$$m_{12} \equiv m(\Lambda\pi^-) \text{ and } m_{13} \equiv m(\Lambda\pi^+).$$

The so-called "Dalitz plot" given in Fig. 4.30 shows the relation between m_{13}^2 and m_{12}^2. The $\Sigma^\pm$ resonances appear as two bands in the Dalitz plot around 1.4 GeV.